

Pharmacophore-Based Virtual Screening and Biological Evaluation of Small Molecule Inhibitors for Protein Arginine Methylation

Juxian Wang,^{†,‡} Limin Chen,^{§,‡} Sarmistha Halder Sinha,^{†,‡} Zhongjie Liang,^{§,||} Huifang Chai,[#] Sakthivel Muniyan,[△] Yu-Wei Chou,[△] Chao Yang,[†] Leilei Yan,[†] You Feng,[†] Keqin Kathy Li,[⊥] Ming-Fong Lin,[△] Hualiang Jiang,[§] Yujun George Zheng,^{*,†} and Cheng Luo^{*,§,||}

[†]Department of Chemistry, Program of Molecular Basis of Diseases, Georgia State University, P.O. Box 4098, Atlanta, Georgia 30302, United States

[§]Drug Discovery and Design Center, State Key Laboratory of Drug Research, Shanghai Institute of Materia Medica, Chinese Academy of Sciences, Shanghai 201203, China

[#]Department of Pharmacy, Guiyang College of Traditional Chinese Medicine, Guiyang 550002, China

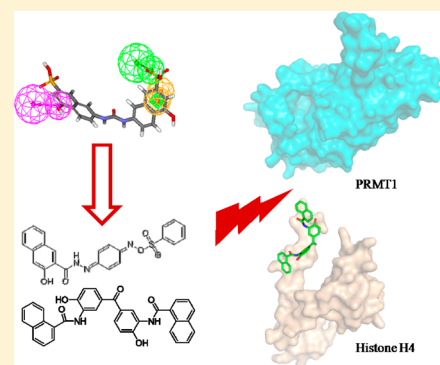
[⊥]State Key Laboratory of Medical Genomics, Shanghai Institute of Hematology, Rui Jin Hospital Affiliated to Shanghai Jiao Tong University School of Medicine, Shanghai, China

^{||}Center for Systems Biology, Soochow University, Jiangsu 215006, China

[△]Department of Biochemistry and Molecular Biology, University of Nebraska Medical Center, Omaha, Nebraska 68198, United States

Supporting Information

ABSTRACT: Protein arginine methyltransferases (PRMTs) are proved to play vital roles in chromatin remodeling, RNA metabolism, and signal transduction. Aberrant regulation of PRMT activity is associated with various pathological states such as cancer and cardiovascular disorders. Development and application of small molecule PRMT inhibitors will provide new avenues for therapeutic discovery. The combination of pharmacophore-based virtual screening methods with radioactive methylation assays provided six hits identified as inhibitors against the predominant arginine methyltransferase PRMT1 within micromolar potency. Two potent compounds, **A9** and **A36**, exhibited the inhibitory effect by directly targeting substrate H4 other than PRMT1 and displayed even higher inhibition activity than the well-known PRMT inhibitors AMI-1. **A9** significantly inhibits proliferation of castrate-resistant prostate cancer cells. Together, **A9** may be a potential inhibitor against advanced hormone-independent cancers, and the work will provide clues for the future development of specific compounds that block the interaction of PRMTs with their targets.



INTRODUCTION

In eukaryotic cells, histones are subject to various posttranslational modifications such as methylation, acetylation, phosphorylation, sumoylation, and ubiquitylation.¹ In particular, the amino-terminal tails of the four core histone proteins are rich in arginine and lysine residues, many of which are found to be heavily methylated. The reaction of methylation is specifically catalyzed by protein arginine methyltransferases (PRMTs). In addition to histones, a large number of non-histone proteins involved in signal transduction and cell proliferation are also shown to contain methyl arginine markers.² The influence of protein arginine N-methylation on cell function is becoming widely appreciated, which involves a host of biological processes including protein trafficking, signal transduction, DNA transcriptional regulation, DNA repair, RNA maturation, embryonic stem cell pluripotency, and embryonic development.^{3–8}

PRMTs can monomethylate and dimethylate the terminal nitrogen atom of guanidinium side chains within arginine residues of proteins using S-adenosyl-L-methionine (SAM or AdoMet) as methyl donor. PRMT1 accounts for 85% of cellular PRMT activity in mammalian cells, which is a predominant PRMT.⁹ Abnormal activity of PRMT1 is associated with various diseases, including mixed lineage leukemia (MLL) and hormone-dependent cancers. PRMT1 is an essential component for oncogenic transformation induced by a MLL complex.³ Direct fusion of MLL with PRMT1 promotes self-renewal of primary hematopoietic cells. On the contrary, specific knock-down of PRMT1 expression suppresses MLL-mediated transformation. PRMT1 is associated with the up-regulation of serum ω-N^G,N^G-asymmetric dimethylarginine (ADMA), which is an

Received: April 12, 2012

Published: August 28, 2012

endogenous nitric oxide synthase (NOS) inhibitor, blocks the production of NO, and causes many cardiovascular implications such as diabetes and hypertension¹⁰ and other implications such as inflammatory reactions.¹¹

PRMT-mediated arginine methylation plays key roles in various biological processes and diseases. However, compared with histone deacetylases (HDACs), the development of arginine methyltransferase inhibitor is still at a slow development stage. In addition to cofactor analogues such as sinefungin,¹² only a few potent arginine methyltransferase inhibitors have been reported^{2,4,13–18} and rarely have been widely recognized. Moreover, current methyltransferase inhibitors, with low specificity, target many other enzymes that use SAM as a cofactor. The sequences among PRMTs throughout evolution are highly conserved, increasing the difficulty of developing potent and specific PRMT inhibitors.

In the past several decades, virtual screening has emerged as a powerful tool for identifying novel compounds with structural diversity,^{19–22} which is a complementary approach to high-throughput screening. It allows the discovery of novel bioactive compounds from very large compound databases through information about either a set of active ligands or the protein active pocket. If the crystal structure of target protein is available, the molecular docking approach is usually carried out. However, the pharmacophore method is an alternative choice when the structure of the target is unknown. The pharmacophore model interprets the interaction between a receptor and a ligand, which is a successful computational drug design approach.²³ Typically, a pharmacophore model was constructed according to the common structural features of existing active compounds. Pharmacophore-based virtual screening has been successfully carried out in the search for novel leads for several targets.^{24–26}

In this study, pharmacophore-based virtual screening was employed for searching novel PRMT1 inhibitors within the SPECS database containing more than 300000 compounds. Pharmacophore models were first constructed on the basis of reported active compounds. Then the top-scored compounds through the pharmacophore-based virtual screening were subjected to cluster analysis; 102 compounds were selected and purchased for further PRMT1 inhibitor bioactivity assay. Experimental results demonstrated that six potential compounds can inhibit PRMT1 activity on the micromolar scale. The two most potent compounds, **A9** and **A36** with similar structures, are found to be more efficacious than previously reported PRMT1 inhibitors AMI-1. Further experimental studies demonstrate that compound **A36** is noncompetitive versus both peptide substrate and SAM, whereas **A9** is competitive versus peptide and noncompetitive versus SAM. Interestingly, both **A9** and **A36** exhibit inhibitory potency for PRMT1 through targeting of the substrates. **A9** significantly inhibits proliferation of prostate cancer cells both in regular culture media and in hormone-depleted media. Taken together, this work provides new lead molecules and structural clues to develop inhibitors that regulate PRMT1-mediated arginine methylation, and **A9** may be a potential therapeutic for treating advanced castration-resistant prostate cancer.

RESULTS AND DISCUSSION

Pharmacophore-Based Virtual Screening. The process for virtual screening in this study is shown in Figure 1. First of all, nine pharmacophore models (Table 1) were constructed based on a training set including 17 reported compounds^{9,17}

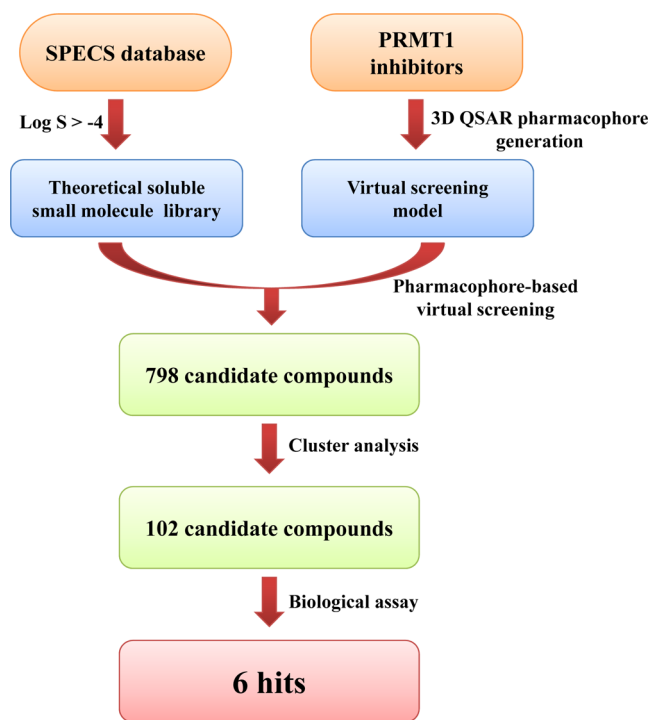


Figure 1. Flowchart for virtually screening PRMT1 inhibitors.

(Supporting Information, Table S1) with a large scale PRMT1 inhibitive bioactivity and structural diversity in Accelrys Discovery Studio 2.1 (Accelrys Inc., San Diego, CA, USA). Typically, two index values were used to evaluate the statistical significance of hypotheses: the margin between null cost and fixed cost, and the margin between null cost and total cost (Δcost). The margin between the null cost and the fixed cost should be >80 . The value indicates the chance of finding useful hypotheses. In this study, the difference between null cost and fixed cost was 87.462. A good hypothesis may usually be obtained when Δcost is >60 . Δcost for all nine hypotheses generated was >85 , indicating 90% statistical significance of these hypotheses (Table 1). Furthermore, the correlation coefficient, >0.9 is often considered good standards for the alignment of the training set compounds with the hypothesis. The correlation coefficient for all nine hypotheses generated is >0.91 (Table 1). In addition, this training set contained two well-recognized PRMT1 inhibitors, AMI-1 and allantodapsonone¹⁷ (Supporting Information, Table S1). AMI-1 and allantodapsonone can map all nine pharmacophore models well (fit value is >4.6), and a few examples of AMI or allantodapsonone fitting the models are shown in Figure S1 of the Supporting Information. Taking these pieces of information together demonstrated that the nine hypotheses generated with statistical significance would be suitable for further virtual screening.

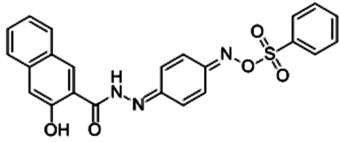
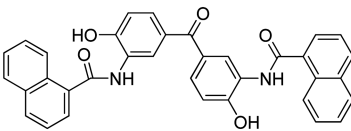
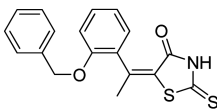
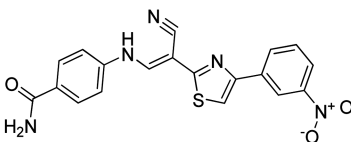
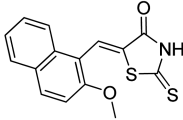
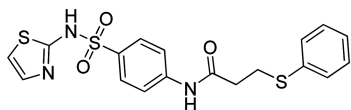
To validate the reliability of the nine constructed pharmacophore models, the pharmacophore models were employed to screen the testing set database. The nine models can efficiently recover the known inhibitors of PRMT1. Models 2–5 achieved higher enrichment ratios than models 6–10 (Supporting Information, Figure S2A). In the meantime, these models were well clustered according to the pharmacophore features (Supporting Information, Figure S2B). Taking these pieces of information together, models 2–5 (colored red in Figure S2B of Supporting Information) from two classes were identified as rational models for virtual screening. Models 2 and

Table 1. Results of Statistical Significance, Correlation Coefficients, and Features of Nine Hypotheses^a

hypothesis	total cost	rms ^b	correlation	Δ cost ^c	features ^{d,e}		
					HBA ^f	HBD	RA
2	80.413	0.385	0.930	86.192	*	*	*
3	80.423	0.388	0.930	86.182	* ²		*
4	80.453	0.392	0.928	86.152	* ²		*
5	80.520	0.401	0.925	86.085	*	*	*
6	80.666	0.423	0.916	85.939	* ²		*
7	80.722	0.414	0.923	85.883	* ²		*
8	80.836	0.433	0.915	85.769	* ²		*
9	80.933	0.433	0.917	85.672	* ²		*
10	81.047	0.438	0.916	85.558	* ²		*

^aFixed cost of nine hypotheses is 79.143, and null cost value is 166.605. ^brms, root-mean-square. For rms value, the smaller, the better. ^c Δ cost = (null cost) – (total cost). ^dHBA, HB_ACCEPTOR; HBD, HB_DONOR; RA, RING_AROMAIC. ^eThe asterisk (*) indicates that these features were present in the hypothesis. ^fNumber of the feature presenting in the hypothesis.

Table 2. Chemical Structures of Identified Small Molecules That Show Inhibitive Activity against PRMT1

Compound ID	SPECS product ID	compound	Inhibition (%)
A9	AE- 848/32000014		65%
A36	AE- 848/34542007		79%
A18	AA- 516/12432333		48%
A56	AE- 848/15341269		51%
A44	AA- 516/33240027		42%
A69	AE- 641/15338016		52%

5 with similar features consist of one HBA, one HBD, and one RA. The features of models 3 and 4 included two HBA and one RA. AMI-1 could map on models 2 and 5 well, and

allantodapson could map on models 3 and 4 well (Supporting Information, Figure S1). AMI-1 and allantodapson are the two most potent compounds within the training set; we concluded

that identified hits based on the four models would have pharmacophore features similar to those of AMI-1 or allantodapson.

Next, the four rational models were chosen as queries against the theoretical soluble SPECS database that contains 90000 small molecule compounds. The amounts of the candidate compounds predicted by each of the four pharmacophore models are summarized in Figure S3A of the Supporting Information. The numbers of candidate compounds acquired from each pharmacophore model were almost equal. Because the four models share several similar features, some compounds screened by different models may be the same. Figure S3B of the Supporting Information is the alignment of the screening results from different pharmacophore models. After deletion of the duplicates, 798 unique candidate compounds were obtained for further research.

Cluster analysis demonstrated that the 798 compounds were divided into 40 groups according to structural features. Compounds in every group were arranged on the basis of fit values, which were results from pharmacophore-based virtual screening; 3 top-ranked compounds were selected from every group, and 120 candidate compounds were selected. However, only 102 compounds were available from the SPECS database for biochemical assay.

Identification of A9 and A36 as PRMT1 Inhibitors by Using Recombinant Enzyme Inhibition Assay. The 102 in silico-screened compounds were tested for inhibitory activity against PRMT1, the predominant arginine methyltransferase in mammalian cells, by using the carbon-14 labeled radioactive methylation assay. In the screening inhibition assay, recombinant histidine-tagged PRMT1 was used as the enzyme and an amino-terminal 20 amino acid H4 peptide (H4–20) was used as the substrate. The methylation products were bound to P81 filter paper and then quantified by liquid scintillation counting. The degree of the decrease in product formation was used as a parameter to evaluate the potency of each compound in inhibiting methyltransferase activity of PRMT1.

From the enzyme inhibition assay, we identified six compounds that inhibited PRMT1 activity by >40% at the concentration of 100 μM (Table 2). The high number of hits validates the accuracy of our pharmacophore-based virtual screening strategy. The hits identified two kinds of pharmacophore models with great structural similarity. On the basis of their structures, these identified inhibitors are characterized as two groups, namely, group I and group II. Group I compounds comprised A9 and A36 that each contain naphthalene aromatic rings and one or two phenolic hydroxyl groups (Table 2). Group II compounds include A18, A44, A56, and A69 that all share a heterocyclic thiazole motif (Table 2). Group I compounds were identified by model 2 or 5, and group II compounds were identified by model 3 or 4. However, group I compounds can inhibit PRMT1 more efficiently than group II compounds. For example, A9 and A36 inhibited 65 and 79% of PRMT activity at the tested concentration. In a more quantitative analysis, we measured the methyltransferase activity of PRMT1 at a range of concentrations of A9 and A36, and the IC_{50} values were derived from the dose response curve as 41.7 and 12.0 μM , respectively. For comparison, we measured IC_{50} of NS-1 and AMI-1 under the same experimental condition, two previously reported PRMT1 inhibitors that also bear naphthalene aromatic rings and phenolic hydroxyl groups.²⁸ It is clear that A9 and A36 showed stronger inhibition for PRMT1 than the well-known inhibitor AMI-1 (Table 3). In particular,

Table 3. Comparison of the Inhibition Activity of A9 and A36 with NSC35605 Stilbamidine and AMI-1

compound	IC_{50} (μM)
A9	41.7 \pm 6.3
A36	12.0 \pm 0.2
NS-1	20.5 \pm 1.7
AMI-1	76.9 \pm 15.4

the potency of A36 is 6-fold that of AMI-1. Our previously discovered inhibitor NS-1 showed similar potency as A9 and A36, but it is structurally more complex and contains two anionic sulfonate groups. Thus its bioavailability may not be as good as A9 and A36. The remarkable potencies of A9 and A36 warrant further investigation of their inhibitory activities and mechanisms.

Inhibition Pattern of Compounds A9 and A36. To provide a molecular basis of PRMT1 inhibition by group I compounds A9 and A36, we performed steady-state kinetics characterization to determine the inhibition pattern of these compounds in PRMT1 catalysis. The initial velocities of PRMT1 were measured at several selected concentrations of each inhibitor over a range of varied concentrations of one substrate while the concentration of the other remained fixed. The data were plotted in the double-reciprocal format with $1/\text{velocity}$ versus $1/[\text{concentration of the varied substrate}]$ (Figure 2). As can be seen from the double-reciprocal plots, in the presence of A9, a series of straight lines intersected on the $1/\text{velocity}$ ordinate when the concentrations of H4–20 were varied, whereas the intersecting point moved to the western side of the ordinate when the concentrations of SAM were varied. These data demonstrate that A9 is competitive versus the peptide substrate and noncompetitive versus the methyl donor SAM (Figure 2A,B). We fitted the primary velocity versus peptide concentration data in the presence of different concentrations of A9 to the nonlinear kinetic equation²⁷ and derived the inhibition constants $K_{\text{is}} = 8.4 \pm 1.8 \mu\text{M}$ and $K_{\text{ii}} > 257 \mu\text{M}$. K_{is} is significantly smaller than K_{ii} , which validates the competitive nature of A9 against H4 substrate. For A36 inhibition, the intersecting points in both $1/v \sim 1/[\text{SAM}]$ and $1/v \sim 1/[\text{H4–20}]$ double-reciprocal plots were found to be in the fourth quadrant, suggesting A36 is a noncompetitive inhibitor with respect to peptide and substrate (Figure 2C,D). A stricter analysis of the primary velocity versus H4 concentration plots yielded $K_{\text{is}} = 11.3 \pm 1.8 \mu\text{M}$ and $K_{\text{ii}} = 29.7 \pm 0.8 \mu\text{M}$. Given that K_{is} is less than K_{ii} , we conclude that A36 is primarily competitive with respect to the H4 substrate. Such a mechanism of action for both A9 and A36 is consistent with that of AMI-1. For A36, the K_{ii} component cannot be neglected, and it likely suggests that A36 also targets a weaker binding site in PRMT1.

Inhibition Mechanism of Compounds A9 and A36. A9 and A36 bear certain pharmacophore features similar to those of the previously reported inhibitors AMI-1 and NS-1 that both target the substrate of PRMT1 rather than the enzyme to execute inhibitory effect.²⁸ Furthermore, the kinetic pattern of PRMT1 inhibition by A9 and A36 suggests that these compounds may compete with peptide substrate. To elucidate the inhibition mechanism, we attempted to test whether A9 and A36 also target the substrate of PRMT1 to execute the inhibitory effect. In this set of experiments, we directly probed the possible binding interaction between A36 and PRMT1 or with the substrate by carrying out spectroscopic measurements.

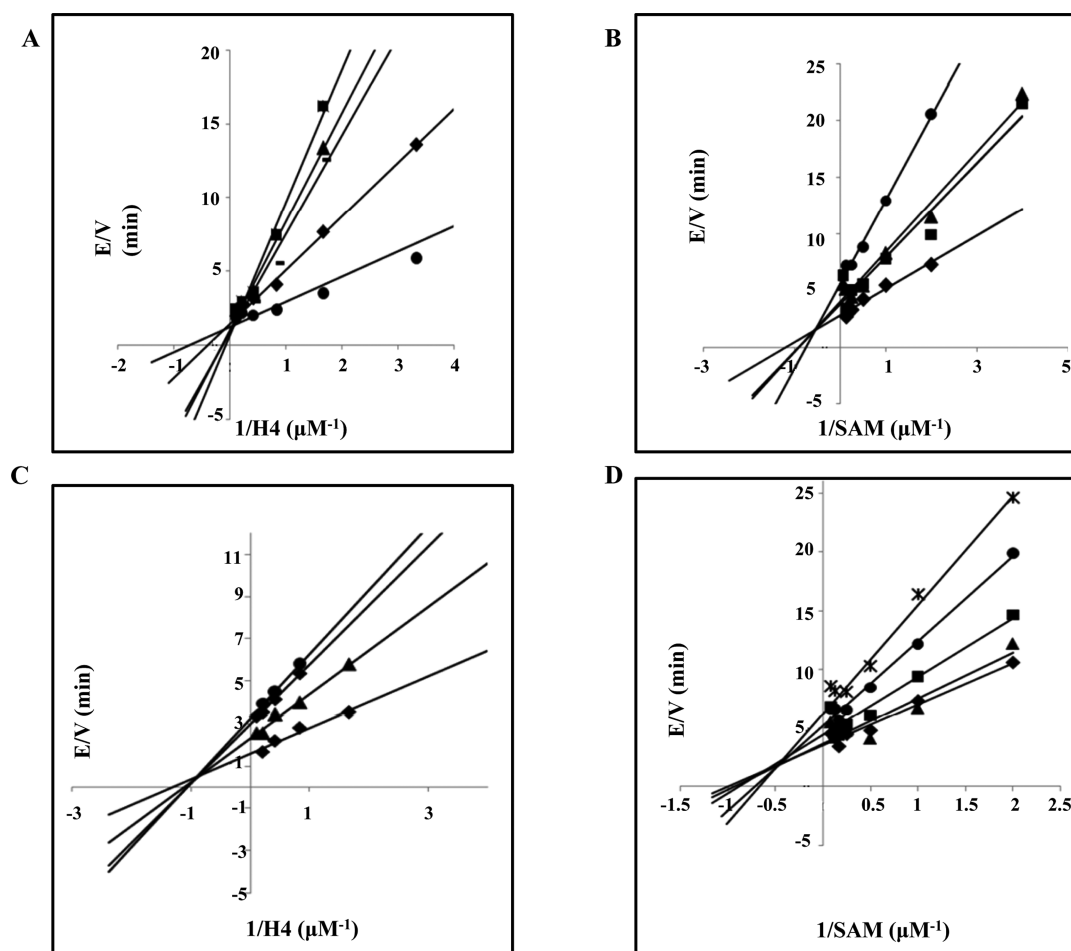


Figure 2. Kinetic analysis of PRMT1 inhibition by A9 and A36: (A) double-reciprocal plotting of initial velocities versus varied concentrations of H4(1–20) at fixed [^{14}C]-SAM (5 μM) and varying A9 [0 μM (\bullet), 20 μM (\blacklozenge), 40 μM ($-$), 60 μM (\blacktriangle), and 80 μM (\blacksquare)]; (B) double-reciprocal plotting of initial velocities versus varied concentrations of [^{14}C]-SAM at fixed H4–20 (2 μM) and varying A9 [0 μM (\blacklozenge), 20 μM (\blacksquare), 40 μM (\blacktriangle), and 80 μM (\bullet)]; (C) double-reciprocal plotting of initial velocities versus varied concentrations of H4–20 at fixed [^{14}C]-SAM (5 μM) and varying A36 [0 μM (\blacklozenge), 10 μM (\blacktriangle), 20 μM (\blacksquare), and 30 μM (\bullet)]; (D) double-reciprocal plotting of initial velocities versus varied concentrations of [^{14}C]-SAM at fixed H4–20 (2 μM) and varying A36 [0 μM (\blacklozenge), 10 μM (\blacktriangle), 20 μM (\blacksquare), 30 μM (\bullet), and 40 μM ($*$)].

For inhibitor–substrate interaction, we collected the fluorescence emission spectra of a fluorescein-labeled H4 peptide, namely H4(1–20)FL with the sequence Ac-SGRGKGGKGDpr(FL)GKGGAKRHRK, in the presence of different concentrations of the inhibitor A36. It was found from the spectra of H4(1–20)FL that the addition of increasing concentrations of A36 significantly quenched the fluorescence emission of H4(1–20)FL (Figure 3A,B). To analyze the enzyme–inhibitor interaction, we measured the intrinsic fluorescence of PRMT1 in the addition of increased concentration of the inhibitor (Figure 3C,D). In contrast, the fluorescence emission of the enzyme was changed very little by the inhibitor. These data strongly suggest that the interaction between A36 and H4(1–20)FL is much stronger than the A36–enzyme interaction (if there is any). From the fluorescence binding measurement, K_d of A36 with the substrate was obtained as 23.8 μM , which is close to the range of its IC_{50} value. We also tried several other biophysical methods to further confirm the binding between A9/A36 and H4 substrate, including ESI-MS, isothermal titration calorimetry (ITC), and surface plasma resonance (SPR). Unfortunately, none of these assays were sensitive enough to detect the interaction (data not shown).

Inhibition of Histone Acetyltransferase (HAT) Activity of p300 by A36.

The observed inhibition of PRMT1 via targeting the substrate indicates that A36 may inhibit the other enzymes that modify the amino-terminal tail of histone H4. To investigate this possibility, we tested the activity of A36 on the acetylation of H4–20 by p300, a well-known HAT enzyme that is able to acetylate the N-terminal tail of H4 at multiple sites.²⁹ The measurement was carried out with 0.03 μM p300, 5 μM [^{14}C]-acetyl CoA, and 10 μM H4–20, at varied concentrations of A36. The dose-dependent assay yielded IC_{50} of 15.2 ± 1.7 μM (Figure 4). Such potency in HAT inhibition is very similar to that of PRMT1 inhibition by A36. These data provide further evidence that A36 binds to H4 directly, preventing H4 from being recognized by histone-modifying enzymes p300 and PRMT1. Thus, A36 targets substrate rather than the enzyme for the inhibition, in the same manner as certain previously reported arginine methylation inhibitors.²⁸

Enzymatic Selectivity of A36. To investigate whether A36 is a selective inhibitor against PRMT1, we compared its inhibitory activity toward PRMT1, PRMT4, and PRMT5 using the radioactive methylation assay. Each reaction mixture contained specified concentrations of recombinant PRMT, [^{14}C] SAM, and peptide substrate and was incubated at 30 $^\circ\text{C}$ in

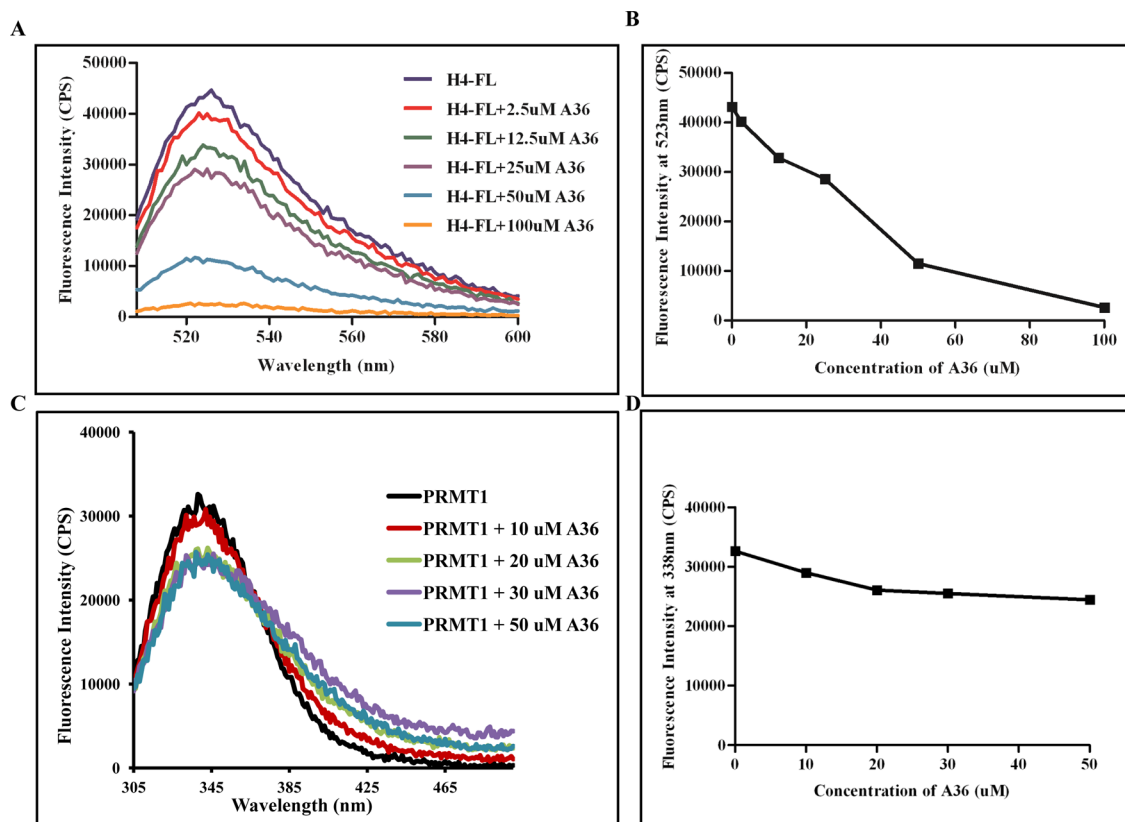


Figure 3. Effect of A36 on the fluorescence spectra of H4(1–20)FL and PRMT1: (A) fluorescence emission spectra of H4(1–20)FL (1 μM) at different concentrations of A36 (0–100 μM) (excitation wavelength = 498 nm); (B) fluorescence intensity of H4(1–20)FL at 523 nm as a function of A36 concentration; (C) fluorescence emission spectra of PRMT1 (1 μM) at different concentrations of A36 (0–50 μM) (excitation wavelength = 285 nm); (D) fluorescence intensity of H4(1–20)FL at 338 nm as a function of A36 concentration.

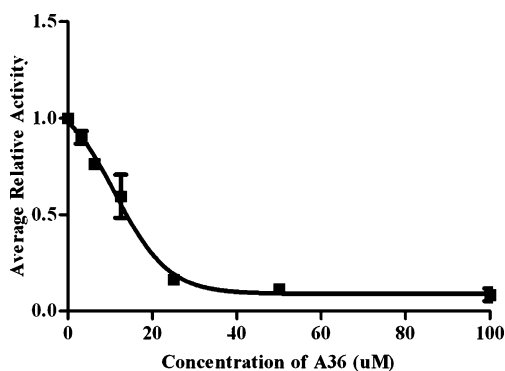


Figure 4. Inhibition of p300 HAT activity by A36. The fractional activity of p300 is plotted with respect to the concentration of A36.

the presence or absence of 30 μM A36. For both PRMT1 and PRMT5 assays, H4–20 was used as the substrate, whereas for the PRMT4 assay H3(1–20) was used as the substrate. The retained activity of each PRMT in the presence of A36 was normalized using its respective controls (no inhibitor) and is presented in Figure 5. It is seen that A36 inhibited PRMT4 activity at a potency 7.5-fold weaker than PRMT1 and inhibited PRMT5 at 2-fold potency weaker than PRMT1. Although PRMT1 and PRMT5 have similar substrate specificities, they undergo different types of methylation, so the minor difference in activity of A36 for PRMT1 and PRMT5 is likely caused by the structural difference between the two proteins. On the other hand, PRMT4 has a distinct substrate specificity from PRMT1, and PRMT4 preferentially methylates histone H3, whereas

PRMT1 preferentially methylates histone H4. Such variation in inhibition potency may be caused either by structural differences between PRMT1 and PRMT4 or by the distinct nature of the substrates used. To sum up, A36 exhibits stronger potency for PRMT1 than PRMT5 and PRMT4.

Effect of A9 and A36 on Prostate Cancer Cell Proliferation.

Because compounds A9 and A36 were identified and characterized as the two most potent compounds for inhibiting PRMT1 activity from the screening study, we further investigated whether these compounds have any effect on the proliferation of disease cells. LNCaP C-81 cells exhibit many biochemical properties of the advanced prostate cancer phenotype, including functional androgen receptor (AR) expression and prostate-specific antigen (PSA) secretion, with rapid growth in the steroid-deprived condition.^{30,31} In regular culture medium, A9 can significantly inhibit the proliferation of LNCaP C-81 cells by up to 70%, following a dose-dependent manner (Figure 6A). Because prostate cancer growth is regulated by steroids, we next investigated whether A9 can also inhibit the proliferation of LNCaP C-81 cells in a steroid-reduced condition, mimicking the clinical androgen-ablation state. As shown in Figure 6B, 10 μM A9 has a significant inhibitory effect on the proliferation of LNCaP C-81 cells by 30%. The structure of A36 is similar to that of A9; however, the effect of A36 on the proliferation of LNCaP C-81 cells is much weaker than that of A9, only about 32% in regular medium (data not shown). Large molecular weight is likely to contribute to the poor biological activity of A36 on cells.

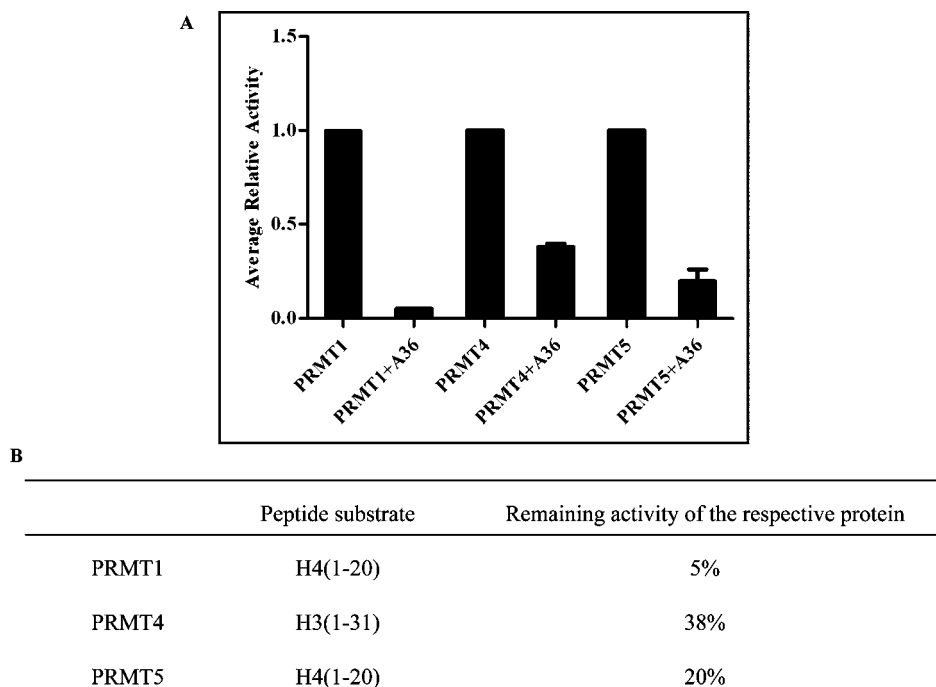


Figure 5. (A) Comparative activity of A36 for PRMT1, PRMT4, and PRMT5. (B) Quantification of remaining activity of respective PRMT.

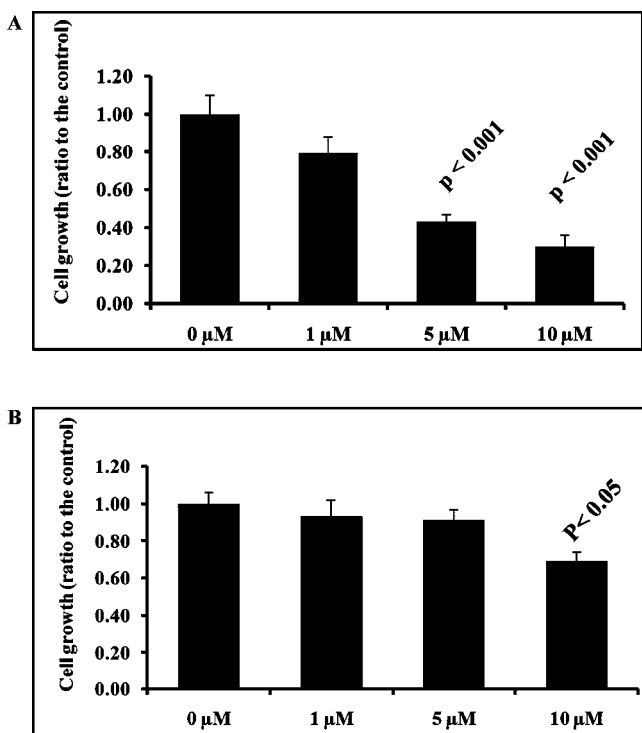


Figure 6. Antiproliferative effect of A9 on prostate cancer cells: (A) dose-dependent effect of A9 on LNCaP C-81 cells in (A) regular medium and (B) steroid-reduced medium. The results presented are the mean \pm SD of three sets of independent experiments in triplicates. $p < 0.05$ and $p < 0.001$ are statistically significant differences from controls.

CONCLUSION

Arginine methylation catalyzed by PRMTs regulates various cellular processes, such as DNA repair, RNA processing, and nucleosomal remodeling. However, the research on developing effective PRMT inhibitors is relatively slow in comparison to

HDAC inhibitor discovery work. Most PRMT inhibitors reported so far have low efficacy and specificity. In this study, by combining pharmacophore-based virtual screening and biochemical methylation assays, we have successfully identified six small molecules that inhibit PRMT1 activity at micromolar potency. Group I compounds, A9 and A36, exhibit the best inhibitory effect with IC_{50} values of 41.7 and 12.0 μ M, respectively, which are more potent than AMI-1 under the same reaction conditions (Table 2). We further conducted steady-state kinetic characterization to determine the inhibition patterns of A9 and A36 in PRMT1 catalysis. Interestingly, the biochemical data demonstrate that the A9 compound is competitive versus peptide substrate and noncompetitive versus SAM, whereas the compound A36 is noncompetitive versus both peptide and SAM. The structures and kinetic patterns of A9 and A36 are similar to that of previously identified PRMT1 inhibitors AMI-1 and NS-1. Indeed, further close examinations showed that A36 also binds to the histone substrate, preventing recognition of the substrate by the enzyme, which is important for the enzymatic activity. A36 also inhibited the activity of p300 that uses H4–20 as a substrate, with an IC_{50} value of 15.2 μ M. This is consistent with the conclusion that A36 binds to the substrate to exhibit enzyme activity. A9 significantly inhibited the proliferation of prostate cancer LNCaP C-81 cells; the effect of A36 is weaker than that of A9. Because PRMT1 catalyzes arginine methylation of diverse proteins, inhibition of the activity of PRMT1 overwhelmingly results in extensive inhibition of methylation of multiple target substrates other than a particular substrate sequence, potentially causing adverse side effects and complications. In this study, we discovered novel inhibitors that target the PRMT1 substrate and regulate PRMT1-mediated histone arginine methylation. Developing new modules of therapies targeting specific genes or gene products is a prominent aim of modern cancer biology. It is of high merit to discover small molecule probes that effectively modulate PRMT-mediated methylation by noncanonical mechanisms. Recently, small molecules targeting histones

were shown to block cancer cell growth both in vitro and in vivo. Thus, **A9** that inhibits PRMT1 activity by targeting the histone substrate and shows a strong blocking effect on the proliferation of prostate cancer cells may be of therapeutic potential for treating advanced castration-resistant prostate cancers. Overall, the discovered histone binders **A9** and **A36** act as new chemical leads to develop improved inhibitors that block the interaction of PRMTs and their histone targets.

EXPERIMENTAL SECTION

Pharmacophore Model Generation and Validation. Seventeen reported compounds with a large scale inhibitive activity against PRMT1 and structural diversity were chosen to generate pharmacophore models in Accelrys Discovery Studio 2.1. During the process of generating pharmacophore models, four chemical features were selected, including HB_ACCEPTOR, HB_DONOR, HYDROPHOBIC, and RING_AROMAIC; CAESAR conformation generation method was chosen; activity uncertainty was set at 3.0; and other control parameters were set at default values.

To validate the accuracy of the pharmacophore models, they were employed to screen the test set database that comprised 27 compounds with PRMT1 inhibition activity and another 183 compounds with structural diversity randomly selected from the SPECS database within Discovery Studio 2.1, respectively. In the meantime, these models were underwent cluster analysis with Discovery Studio 2.1.

Database Preparation and Pharmacophore-Based Screening. The SPECS database from the ZINC database containing more than 300,000 small molecule compounds was filtered with $\log S > -4$ to construct a theoretical soluble SPECS database. Four rational pharmacophores were conducted to screen the theoretical soluble SPECS database with flexible search method within Discovery Studio 2.1 one by one. During the screening process, the CAESAR conformation generation method was used, and the maximum number of conformers generated was set to 250; other control parameters were set as default values.

Small Molecule Compounds. Small molecule organic compounds were purchased from SPECS Corp. (The Netherlands).

Peptide Substrates. Peptides were synthesized following the standard solid phase peptide synthesis (SPPS) protocols, purified with C-18 reversed phase HPLC, and confirmed with MALDI-MS as previously described.³² The structural sequence of the NH₂-terminal peptide of histone H4, H4-20, is Ac-SGRGKGGKGLGKGGAKRHRK. The structural sequence of the NH₂-terminal peptide of histone H3, H3(1-20), is Ac-ARTKQ-TARKSTGGKAPRKQL.

Protein Expression and Purification. His6x-tagged PRMT1 was expressed from the pET28b vector. GST-PRMT1 is expressed from the PGEX4T1 vector. The proteins were expressed in *Escherichia coli* BL21 (DE3). His6x-tagged protein was purified on Ni-NTA beads. Protein concentrations were determined using the Bradford assay.

Radioactive Methylation Assay. The inhibition effect of small molecule compounds was tested using the carbon-14 labeled radioactive methylation assay as previously reported.²⁸ The assays were carried out in 0.6 mL plastic tubes at 30 °C in a reaction volume of 30 μ L. The reaction buffer contained 50 mM HEPES (pH 8.0), 10 mM NaCl, and 1 mM DTT. In a typical inhibition assay, 2 μ M peptide substrate, 5 μ M [¹⁴C]-SAM, and varied concentrations of inhibitor were preincubated in the reaction buffer for 5 min at 30 °C prior to the initiation of the reaction by the addition of enzyme (0.1 μ M final). After incubating for an appropriate period of time (8 min), the reaction was quenched by spreading the reaction mixture onto the surface of P81 filter paper (Whatman). The paper disk was then washed with 50 mM NaHCO₃ (3 \times 300 mL) and dried for 2 h. The amount of methylated products was quantified by liquid scintillation counting.

The inhibition pattern analysis of **A9** and **A36** was determined by measuring initial velocities of PRMT1 at varied concentrations of one substrate, a fixed concentration of the other substrate, and selected concentrations of the inhibitors; 0.1 mM His6x-PRMT1 was used in all

of these assays. The data were displayed in double-reciprocal formats and fitted to competitive or noncompetitive kinetic equations.

Selectivity Test of A36 with Different PRMTs. To know whether **A36** is more selective toward PRMT1 than other PRMT members, a radioactive methylation assay was performed. His6x-rPRMT1, -4, and -5 proteins were expressed in *E. coli* BL21 (DE3). In this assay for three sets of reactions, H4(1-20) for PRMT1 and PRMT5 (2 μ M), H3(1-31) for PRMT4 (400 μ M), and [¹⁴C]-S-adenosyl-L-methionine (5 μ M) were preincubated in the reaction buffer for 5 min prior to the initiation by the addition of PRMT1 (0.05 μ M final), PRMT5 (1 μ M final), and PRMT4 (0.3 μ M final), in the absence of inhibitor. The reaction time used for PRMT1 was 20 min, that for PRMT5 was 6 h and 30 min, and that for PRMT4 was 2 h. At the appropriate time, the reaction was quenched by spreading the reaction mixture onto P81 filter paper disks (Whatman). The paper disk was washed with 50 mM NaHCO₃ (3 \times 300 mL) and dried in air for 2 h. The amount of methylated products was quantified by liquid scintillation. Another three sets of reaction were done in the presence of 30 μ M **A36** and DMSO (2%) by following the same procedure as described above.

Fluorescent Binding Assay. The fluorescence intensity of fluorescein-labeled peptides was measured on a Fluoromax-4 spectrofluorometer (Horiba Jobin Yvon). The buffer was the same as that for the radioactive assay. The excitation and emission wavelengths were selected at 498 and 524 nm, respectively. Fluorescence intensity changes of H4(1-20)FL and PRMT1 at different concentrations of **A36** were measured to detect their interaction. One micromolar concentrations of H4(1-20)FL and PRMT1 at 30 °C were titrated with increasing concentration of **A36** (1-100 μ M for H4(1-20)FL and 1-50 μ M for enzyme interaction) in different sets of experiment.

Inhibition of p300 by A36. Recombinant p300HAT domain (1287-1666) was a gift from Dr. Philip Cole at Johns Hopkins University, and its expression was described in an earlier paper.²⁹ The enzymatic activity of p300 and its inhibition by **A36** were measured by radioactive acetylation assays. A reaction mixture of 10 μ M H4-20, 5 μ M [¹⁴C]-acetyl CoA, 0.03 μ M p300, and increasing concentrations of the inhibitors was incubated in the reaction buffer [50 mM HEPES (pH 8.0), 50 mM NaCl, 0.5 mM DTT, and 1 mM EDTA] at 30 °C for 10 min, and the reaction was quenched by loading the mixture onto p81 filter paper. The radioactive products were quantified by liquid scintillation, and the fractional activity of p300 was plotted with respect to the concentration of inhibitors.

Cell Culture and Cell Proliferation assay. RPMI 1640 medium, gentamicin, and trypsin/EDTA reagents were purchased from Invitrogen Corp. (Carlsbad, CA, USA). Regular and charcoal/dextran-treated certified FBS were from Atlanta Biologicals (Lawrenceville, GA, USA). Human prostate carcinoma cell line LNCaP was originally purchased from the American Type Culture Collection (Rockville, MD, USA). LNCaP cells were routinely maintained in the regular medium, that is, phenol red-positive RPMI 1640 medium supplemented with 5% FBS, 2 mM glutamine, and 50 μ g/mL gentamicin. The LNCaP PCa cell progression model was described originally by Lin et al.³⁰ and further characterized by Igawa et al.³¹ with passage numbers between 80 and 120 as C-81. For steroid-reduced (SR) medium, cells were maintained in phenol red-free RPMI 1640 medium containing 5% charcoal/dextran-treated FBS (v/v), 2 mM glutamine, 50 μ g/mL gentamicin, and 1 nM dihydrotestosterone (DHT). The cells were maintained at 37 °C in a humidified atmosphere of 5% CO₂ in a CO₂ incubator. **A9** and **A36** were dissolved in DMSO as 1000 \times concentrated stock solutions, stored at -20 °C, and diluted in the respective culture media at the time of use. Control cells were treated with media containing an equal concentration of DMSO.

For the cell proliferation assay, in regular medium, LNCaP C-81 cells were plated at a density of 2×10^3 cells/well in six wells for 3 days and then treated with different concentrations of **A9** or **A36** for 3 days. The cell numbers were counted using a Cellometer Auto T4 Image-based cell counter (Nexcelom Bioscience). The ratio of cell growth was calculated by normalizing the cell number to that of the control cells. In SR medium condition, C-81 cells were plated as described above for 3 days and then steroid-starved for 2 days in a SR medium. After feeding

with fresh SR medium, cells were treated with different concentrations of A9 or A36 for 3 days. Control cells were treated with solvent alone. The cell numbers were counted, and the ratio of cell growth was calculated by normalizing the cell number to that of the control cells. Results shown are an average of three sets of independent experiments performed in triplicates.

■ ASSOCIATED CONTENT

Supporting Information

Additional experimental data, figures, and graphs. This material is available free of charge via the Internet at <http://pubs.acs.org>.

■ AUTHOR INFORMATION

Corresponding Author

*(C.L.) Phone: +86-21-50271399. Fax: +86-21-50807088. E-mail: clu@mail.shcnc.ac.cn. (Y.G.Z.) Phone: 1-404-413-5491. Fax: 1-404-413-5505. E-mail: yzheng@gsu.edu.

Author Contributions

[‡]These authors contributed equally to this work.

Notes

The authors declare no competing financial interest.

■ ACKNOWLEDGMENTS

We gratefully acknowledge financial support from the National Institutes of Health (NIH), the American Heart Association, and Georgia Cancer Coalition Distinguished Cancer Scholar Award to Y.G.Z. This study was also supported in part by CA88184 (NIH) to M.F.L. We also gratefully acknowledge financial support from State Key Program of Basic Research of China Grant 2009CB918502 to H.J., National Natural Science Foundation of China Grants (20972174, 91029704, 81270622, and 21210003) to C.L., H.J., and K.L., the National High Technology Research and Development Program of China (2012AA020302), and the Chinese Academy of Sciences (XDA01040305) to C.L.

■ ABBREVIATIONS USED

PRMT, protein arginine N-methyltransferase; SAM/AdoMet, S-adenosyl-L-methionine; MLL, mixed lineage leukemia; ADMA, ω -N^G,N^G-asymmetric dimethylarginine; NOS, nitric oxide synthase; HDAC, histone deacetylases; HAT, histone acetyltransferase; AR, androgen receptor; PSA, prostate-specific antigen

■ REFERENCES

- (1) Schäfer, S.; Jung, M. Chromatin modifications as targets for new anticancer drugs. *Arch. Pharm. (Weinheim, Ger.)* **2005**, *338*, 347–357.
- (2) Bedford, M. T.; Richard, S. Arginine methylation: an emerging regulator of protein function. *Mol. Cell* **2005**, *18*, 263–272.
- (3) Cheung, N.; Chan, L. C.; Thompson, A.; Cleary, M. L.; So, C. W. E. Protein arginine-methyltransferase-dependent oncogenesis. *Nat. Cell Biol.* **2007**, *9*, 1208–1215.
- (4) Cheng, D.; Yadav, N.; King, R. W.; Swanson, M. S.; Weinstein, E. J.; Bedford, M. T. Small molecule regulators of protein arginine methyltransferases. *J. Biol. Chem.* **2004**, *279*, 23892–23899.
- (5) Dery, U.; Coulombe, Y.; Rodrigue, A.; Stasiak, A.; Richard, S.; Masson, J.-Y. A glycine-arginine domain in control of the human MRE11 DNA repair protein. *Mol. Cell Biol.* **2008**, *28*, 3058–3069.
- (6) Torres-Padilla, M. E.; Parfitt, D. E.; Kouzarides, T.; Zernicka-Goetz, M. Histone arginine methylation regulates pluripotency in the early mouse embryo. *Nature* **2007**, *445*, 214–218.
- (7) Yu, Z.; Vogel, G.; Coulombe, Y.; Dubeau, D.; Spehalski, E.; Hebert, J.; Ferguson, D. O.; Masson, J. Y.; Richard, S. The MRE11

GAR motif regulates DNA double-strand break processing and ATR activation. *Cell Res.* **2012**, *22*, 305–320.

(8) Lu, J.; Kong, X.; Luo, C.; Li, K. K. Application of epigenome-modifying small molecules in induced pluripotent stem cells. *Med. Res. Rev.* **2012**, DOI: 10.1002/med.21265.

(9) Heinke, R.; Spannhoff, A.; Meier, R.; Trojer, P.; Bauer, I.; Jung, M.; Sippl, W. Virtual screening and biological characterization of novel histone arginine methyltransferase PRMT1 inhibitors. *Chem. Med. Chem.* **2009**, *4*, 69–77.

(10) Sasser, J. M.; Moningka, N. C.; Cunningham, M. W.; Croker, B.; Baylis, C. Asymmetric dimethylarginine in angiotensin II-induced hypertension. *Am. J. Physiol.* **2010**, *298*, 740–746.

(11) Chen, M. F.; Xie, X. M.; Yang, T. L.; Wang, Y. J.; Zhang, X. H.; Luo, B. L.; Li, Y. J. Role of asymmetric dimethylarginine in inflammatory reactions by angiotensin II. *J. Vasc. Res.* **2007**, *44*, 391–402.

(12) Vedel, M.; Lawrence, F.; Robert-Gero, M.; Lederer, E. The antifungal antibiotic simefungin as a very active inhibitor of methyltransferases and of the transformation of chick embryo fibroblasts by rous sarcoma virus. *Biochem. Biophys. Res. Commun.* **1978**, *85*, 371–376.

(13) Ragno, R.; Simeoni, S.; Castellano, S.; Vicidomini, C.; Mai, A.; Caroli, A.; Tramontano, A.; Bonaccini, C.; Trojer, P.; Bauer, I.; Brosch, G.; Sbardella, G. Small molecule inhibitors of histone arginine methyltransferases: homology modeling, molecular docking, binding mode analysis, and biological evaluations. *J. Med. Chem.* **2007**, *50*, 1241–1253.

(14) Mai, A.; Cheng, D.; Bedford, M. T.; Valente, S.; Nebbioso, A.; Perrone, A.; Brosch, G.; Sbardella, G.; De Bellis, F.; Miceli, M.; Altucci, L. Epigenetic multiple ligands: mixed histone/protein methyltransferase, acetyltransferase, and class III deacetylase (sirtuin) inhibitors. *J. Med. Chem.* **2008**, *51*, 2279–2290.

(15) Zheng, Y. G.; Wu, J.; Chen, Z.; Goodman, M. Chemical regulation of epigenetic modifications: opportunities for new cancer therapy. *Med. Res. Rev.* **2008**, *28*, 645–687.

(16) Li, K. K.; Luo, C.; Wang, D.; Jiang, H.; Zheng, Y. G. Chemical and biochemical approaches in the study of histone methylation and demethylation. *Med. Res. Rev.* **2012**, *32*, 815–867.

(17) Spannhoff, A.; Heinke, R.; Bauer, I.; Trojer, P.; Metzger, E.; Gust, R.; Schule, R.; Brosch, G.; Sippl, W.; Jung, M. Target-based approach to inhibitors of histone arginine methyltransferases. *J. Med. Chem.* **2007**, *50*, 2319–2325.

(18) Bissinger, E.-M.; Heinke, R.; Spannhoff, A.; Eberlin, A.; Metzger, E.; Cura, V.; Hassenboehler, P.; Cavarelli, J.; Schüle, R.; Bedford, M. T.; Sippl, W.; Jung, M. Acyl derivatives of *p*-aminosulfonamides and dapsons as new inhibitors of the arginine methyltransferase hPRMT1. *Bioorg. Med. Chem.* **2011**, *19*, 3717–3731.

(19) Stahl, M.; Guba, W.; Kansy, M. Integrating molecular design resources within modern drug discovery research: the Roche experience. *Drug Discov. Today* **2006**, *11*, 326–333.

(20) Liang, Z.; Zhang, D.; Ai, J.; Chen, L.; Wang, H.; Kong, X.; Zheng, M.; Liu, H.; Luo, C.; Geng, M.; Jiang, H.; Chen, K. Identification and synthesis of *N'*-(2-oxoindolin-3-ylidene)hydrazide derivatives against c-Met kinase. *Bioorg. Med. Chem. Lett.* **2011**, *21*, 3749–3754.

(21) Luo, C.; Xie, P.; Marmorstein, R. Identification of BRAF inhibitors through in silico screening. *J. Med. Chem.* **2008**, *51*, 6121–6127.

(22) Li, N.; Thompson, S.; Schultz, D. C.; Zhu, W.; Jiang, H.; Luo, C.; Lieberman, P. M. Discovery of selective inhibitors against EBNA1 via high throughput in silico virtual screening. *PLoS One* **2010**, *5*, 1–9.

(23) Guner, O.; Clement, O.; Kurogi, Y. Pharmacophore modeling and three dimensional database searching for drug design using catalyst: recent advances. *Curr. Med. Chem.* **2004**, *11*, 2991–3005.

(24) Dube, D.; Periwal, V.; Kumar, M.; Sharma, S.; Singh, T.; Kaur, P. 3D-QSAR based pharmacophore modeling and virtual screening for identification of novel pteridine reductase inhibitors. *J. Mol. Model.* **2011**, 1–11.

(25) Tanneeru, K.; Guruprasad, L. Ligand-based 3-D pharmacophore generation and molecular docking of mTOR kinase inhibitors. *J. Mol. Model.* **2011**, 1–14.

(26) Chen, Z.; Tian, G.; Wang, Z.; Jiang, H.; Shen, J.; Zhu, W. Multiple pharmacophore models combined with molecular docking: a reliable way for efficiently identifying novel PDE4 inhibitors with high structural diversity. *J. Chem. Inf. Model.* **2010**, 50, 615–625.

(27) Wu, J.; Xie, N.; Wu, Z.; Zhang, Y.; Zheng, Y. G. Bisubstrate inhibitors of the MYST HATs Esa1 and Tip60. *Bioorg. Med. Chem.* **2009**, 17, 1381–1386.

(28) Feng, Y.; Li, M.; Wang, B.; Zheng, Y. G. Discovery and mechanistic study of a class of protein arginine methylation inhibitors. *J. Med. Chem.* **2010**, 53, 6028–6039.

(29) Thompson, P. R.; Kurooka, H.; Nakatani, Y.; Cole, P. A. Transcriptional coactivator protein p300. *J. Biol. Chem.* **2001**, 276, 33721–33729.

(30) Lin, M.-F.; Meng, T.-C.; Rao, P. S.; Chang, C.; Schönthal, A. H.; Lin, F.-F. Expression of human prostatic acid phosphatase correlates with androgen-stimulated cell proliferation in prostate cancer cell lines. *J. Biol. Chem.* **1998**, 273, 5939–5947.

(31) Igawa, T.; Lin, F.-F.; Lee, M.-S.; Karan, D.; Batra, S. K.; Lin, M.-F. Establishment and characterization of androgen-independent human prostate cancer LNCaP cell model. *Prostate* **2002**, 50, 222–235.

(32) Xie, N.; Elangwe, E. N.; Asher, S.; Zheng, Y. G. A dual-mode fluorescence strategy for screening HAT modulators. *Bioconjugate Chem.* **2009**, 20, 360–366.